Plant Soil (2016) 401:7–22
DOI 10.1007/s11104-015-2494-5

REGULAR ARTICLE

Phosphorus speciation and micro-scale spatial distribution in North-American temperate agricultural soils from micro X-ray fluorescence and X-ray absorption near-edge spectroscopy

Camille Rivard · Bruno Lanson · Marine Cotte

Received: 30 December 2014 / Accepted: 22 April 2015 / Published online: 10 May 2015

Abstract
Background and Aims Phosphorus (P) is an essential nutrient for plants but its low availability often necessitates amendments for agronomical issues. Objectives were to determine P spatial distribution and speciation that remain poorly understood in cultivated soils.
Methods Aquic Argiudoll soil samples developed on a calcareous loam glacial till were collected from experimental plots submitted to contrasting crop rotations and amendments. Micro-X-ray fluorescence (μ-XRF) maps were collected on undisturbed samples. X-ray absorption near edge structure (XANES) spectra were collected on bulk samples and on fractions thereof, and on points of interests selected from μ-XRF maps. Results were compared with chemical analyses and extraction techniques results.
Results Chemical analyses show variations in total and exchangeable P contents depending on the samples but no significant difference is observed in terms of P distribution and speciation. P distribution is dominated by a low-concentration diffuse background with a minor contribution from minute hot spots. P speciation is dominated by phosphate groups bound to clay-humic complexes. No modification of P distribution and speciation is observed close to roots.
Conclusions This study evidenced minor effect of cropping and fertilizing practices on P speciation in cultivated soils. Despite analytical challenges, the combined use of μ-XRF and XANES provides relevant information on P speciation in heterogeneous soil media.

Keywords Phosphorus (P) · Speciation · Distribution · Agricultural soil · Micro-X-ray fluorescence (μ-XRF) · X-ray absorption near edge structure (XANES)

Abbreviations

CBD	citrate-bicarbonate-dithionite
CC	continuous corn crops
C-O-H	corn, oats, and hay rotation
DOM	dissolved organic matter
ICP-OES	inductively coupled plasma optical emission spectroscopy
M-NPK	NPK amended plot since 1955 (manure amended between 1904 and 1955)
MPS	manure amended plot since 1904
NOM	natural organic matter

Responsible Editor: Benjamin L. Turner .

Electronic supplementary material The online version of this article (doi:10.1007/s11104-015-2494-5) contains supplementary material, which is available to authorized users.

C. Rivard (✉) · M. Cotte
European Synchrotron Radiation Facility (ESRF),
F-38000 Grenoble, France
e-mail: rivard.camille@gmail.com

B. Lanson
Université Grenoble Alpes, ISTerre, F-38041 Grenoble, France

B. Lanson
CNRS, ISTerre, F-38041 Grenoble, France

M. Cotte
CNRS, LAMS, F-75005 Paris, France

NMR	nuclear magnetic resonance
NPK	nitrogen phosphorus potassium amended plot
POI	point of interest
SNR	signal-to-noise ratio
U	unamended plot
U-NPK	NPK amended plot since 1955 (unamended between 1904 and 1955)
XANES	X-ray absorption near-edge structure
XRD	X-ray diffraction
XRF	X-ray fluorescence
μ-XANES	micro-X-ray absorption near-edge structure
μ-XRF	micro-X-ray fluorescence

Introduction

As an essential plant nutrient, Phosphorus (P) plays a pivotal role in plant root development and in their resistance to exterior stresses. Despite its ubiquity in soils at levels typically ranging 500–1000 ppm, P often appears as a limiting factor for plant growth owing to its low availability. Concentration of P in soil solution (mainly as $H_2PO_4^-$ and HPO_4^{2-} anions, that are hereafter referred to as phosphate together with PO_4^{3-} anions), which is readily available for plant uptake, is indeed 4–5 orders of magnitude lower than in bulk soil. Most of soil P is either included in the structure of organic and inorganic (minerals) compounds or bound (as phosphate groups) at the surface thereof. Dissolution and desorption rates thus exert a strong control on the release of the plant-available P pool, which is commonly assessed with a variety of tests and represents a few percents of the bulk soil P. Low availability of P present in soils often requires supplementary application of P, either as chemical fertilizers or as animal manure, to agricultural land, and especially to acidic soils in an effort to improve crop growth and yield. In chemical fertilizers, P is present mostly as moderately soluble Ca-, NH_4-, urea- or K-phosphate minerals (Hesterberg 2010). As a counterpart to the beneficial effect on soil fertility and crop production, excessive P inputs are detrimental to the environment (e.g., destabilization and eutrophication of natural aquatic environments). A detailed understanding of P distribution and speciation in soils and of the fate of fertilizers is therefore key to optimizing P-supply levels and forms and thus to the sustainable management of P in agricultural lands.

A variety of chemical methods is commonly used on powdered soil samples to determine total- and plant-available- (extractible-) P levels: Mehlich, Ca-chloride, Egner, Bray, and Olsen extraction methods, and their contrasting relative efficiencies have been amply compared as a function of soil characteristics such as pH or calcium abundance (Irving and McLaughlin 1990; Matejovic and Durackova 1994). To assess the different P pools several protocols of sequential fractionation have been developed and refined (e.g., Hedley et al. 1982), usually from the initial protocol of Chang and Jackson (1957), and their selectivity and efficiency compared (Ruban et al. 1999; Tiyapongpattana et al. 2004; Wang et al. 2013). Additional extraction techniques were specifically designed to investigate inorganic P pools (Oxmann et al. 2008). All the above techniques require powdered samples for efficiency, thus intrinsically losing spatial information. In addition these techniques systematically rely on an indirect estimate of the different pools and results may be strongly biased by reactant efficiency and selectivity. Solid-state ^{31}P nuclear magnetic resonance (NMR) spectroscopy, can been used to overcome the latter limitation (Lookman et al. 1996; McDowell et al. 2002). Minimization of sample heterogeneity requires grinding the sample, however (Doolette and Smernik 2011) and analysis is limited to Fe-poor soils (Cade-Menun 2005).

More recently, synchrotron techniques and in particular X-ray Absorption Near-Edge Structure (XANES) spectroscopy have been used to gain direct insight into P speciation in soils, sediments, or manures (Hesterberg et al. 1999; Peak et al. 2002, 2012; Beauchemin et al. 2003; Sato et al. 2005; Lombi et al. 2006; Shober et al. 2006; Brandes et al. 2007; Güngör et al. 2007; Kruse and Leinweber 2008; Lombi and Susini 2009; Negassa et al. 2010; Kar et al. 2012; Giguet-Covex et al. 2013; Liu et al. 2013; Prietzel et al. 2013; Abdala et al. 2015; Eriksson et al. 2015; Kruse et al. 2015). P K-edge XANES spectra can be collected on a variety of samples, with only minor limitations as to their bulk composition. The pre-edge, edge, and post-edge features are characteristic of the local environment of the element (Lombi and Susini 2009). XANES spectra are thus specific to elementary P-bearing components, or at least to a group of chemically and structurally similar components, allowing in particular

differentiation of inorganic and organic P species. Identification of species usually relies on the comparison of experimental spectra with those obtained on P-bearing references, and relative proportions of the P-bearing phases can be determined from linear combination fit to the data. Over the last few years, the development of micro-focused beamlines (with X-ray beams <1 μm in diameter) has allowed development of spatially resolved P XANES spectroscopy (Lombi et al. 2006; Brandes et al. 2007; Giguet-Covex et al. 2013). Despite early technical difficulties, combination of micro X-ray fluorescence (μ-XRF) to determine co-localization of P with other elements with μ-XANES spectroscopy proved extremely useful to identify P-bearing species present in a heterogeneous sample, including minor ones. In addition, achievable detection limits allow investigations on representative agricultural soils.

In the present study we propose to take advantage of the few hundreds ppm detection limits currently achievable with micro-focused setups to determine P distribution and speciation in a set of agricultural soils samples, by combining XRF mapping and XANES spectroscopy techniques using both unfocused (200 μm) and focused (<1 μm) beams. Soil samples were selected from the experimental Morrow Plots (Univ. of Illinois, Urbana-Champaign campus) whose cropping practices have been recorded for ~150 years. Plots with two crop rotations and four types of fertilizer inputs were selected to assess the influence of both cropping and fertilizing practices. Results from X-ray spectroscopic analyses (μ-XRF and XANES) are compared with those from chemical analyses, extraction techniques, and sample fractionation in an effort to determine the average speciation of soil P, its distribution between organic and mineral soil components, and its spatial distribution. Additional information relative to the fate of fertilizer inputs is also sought.

Material and methods

Soil sample collection

Soil samples were collected from the Morrow Plots that are located on the Urbana-Champaign campus of the University of Illinois. Climate is typically continental with cold winters (1981–2014 average low temperatures ranging −7.9 to −5.3 °C in Dec–Feb[1]), warm summers (1981–2014 average high temperatures ranging 28.2 to 29.7 °C in Jun-Aug), and frequent short fluctuations in temperature, humidity, cloudiness, and wind direction. Annual precipitations average ~1035 mm (1981–2014) with ~610 mm snowfalls essentially from Dec-Feb. Soil is an Aquic Argiudoll developed on a calcareous loam glacial till under prairie vegetation. Basic physical and chemical data are reported in Table 1. The Morrow plots are the oldest agricultural experimental plots in the United States (Aref and Wander 1998) and have been cultivated since 1876 with a continuous record of the type of crops, crop rotations, and fertilizer inputs. Out of the ten initial plots, three are still active with 1) continuous-corn crop (plot #3, hereafter referred to as CC plot), 2) a 2-year corn and soybean rotation (not studied here), and 3) a 3 year corn, oats, and hay rotation (plot #5, hereafter referred to as C-O-H plot). Samples were selected from CC and C-O-H plots for the present study. Each of the main plots is divided in eight subplots corresponding to different amendments, essentially manure and NPK at different input levels since 1955 (Aref and Wander 1998). Specifically, four subplots were sampled: the first one (U) was left unamended since 1876, a second one has been fertilized with manure since 1904 (MPS), whereas the other two have been fertilized with NPK since 1955. U-NPK subplot had not been amended before 1955, whereas M-NPK was fertilized with manure, prior to NPK, from 1904 to 1954 (Aref and Wander 1998). Since 1955, seed density is higher in fertilized subplots compared to unamended ones (Aref and Wander 1998). Soil pH was measured on 1:1 soil:water samples with a glass electrode. Mean values obtained from samples collected annually from 1969 to 1995 are significantly lower in unamended subplots compared to amended ones [5.40 and 5.55 for CC/U and C-O-H/U, respectively, compared to 6.19–6.50 for fertilized subplots – Aref and Wander (1998)].

Samples were collected from both CC and C-O-H plots in late September 2012 after corn harvest. To preserve soil texture, mottles of undisturbed soils were cored (9 cm diameter, 3 cm height) at 15–20 cm depth close to maize roots, and capped after sampling in addition to bulk soil sampling at similar depths. Two unamended soil samples from 1904 were also obtained, as slightly ground powders, from the soil library of the Department of Agriculture. Sample names and origins are detailed in Table 2.

[1] http://www.weather.gov/climate/xmacis.php?wfo=ilx

Table 1 Physical and chemical properties of a soil profile on the Morrow Plots [unamended plot with continuous corn crop – adapted from Odell et al. (1982)]

Horizon	Depth (cm)	Granulometry			Organic C (%)	pH	Base saturation (%)	CEC (meq / 100 g soil)	Exchangeable cations (meq / 100 g soil)			
		Sand (%)	Silt (%)	Clay (%)					Ca	Mg	K	Na
Ap	0–23	9.0	66.8	24.2	1.32	5.1	65	17.6	8.8	2.3	0.2	0.1
A12	23–30	8.4	64.8	26.8	1.49	5.3	71	18.0	9.7	2.7	0.2	0.1
B1	30–38	5.6	58.7	35.7	1.20	6.0	83	23.1	13.4	5.5	0.1	0.1
B21t	38–56	5.2	54.8	40.0	0.62	6.2	90	26.0	15.8	7.5	0.1	0.1
B22t	56–76	7.6	57.6	34.8	0.54	6.7	92	22.7	13.6	7.1	0.1	0.1
B3	76–124	12.7	60.9	26.4	0.24	7.5	100	16.8	11.2	5.8	0.1	0.1
IIC1	124–147	26.7	57.1	16.2	0.21	8.1	–	–	–	–	–	–
IIC2	147–183	26.4	55.6	18.0	0.13	8.3	–	–	–	–	–	–

Soil sample preparation

Soil cores were impregnated under vacuum with high-purity polyester resin to prepare micro-polished petrographic thin sections ~30 μm thick. The use of Canada balsam allowed removal of the supporting glass slide and preparation of self-supporting thin sections that were used for μ-XRF and μ-XANES analyses.

Bulk soil samples and remnants from core samples were used both to prepare samples for bulk analyses and to extract various clay-size fractions. Bulk soil samples were first freeze-dried, ground roughly for homogenization, and finely for further analysis. Bulk soil samples were used for X-ray diffraction (XRD), chemical analyses and bulk XANES analyses. Clay-size fractions (<2, 0.2–0.05, and <0.05 μm) were obtained by centrifugation from Na-saturated aliquots of initial soil samples. Initial Na-saturation was performed by shaking bulk samples in a 1 M NaCl solution for 24 h. This initial treatment aimed at enhancing the extraction of the clay-sized fraction and allowed for example recovering ~37 % of sample 3NB in the <2 μm fraction compared to ~29 % when starting from an untreated sample. Aliquots of the clay-size fractions were then treated with a Na-citrate-bicarbonate-dithionite solution (CBD) to remove iron oxides and subsequently with hydrogen peroxide to oxidize organic matter. Both treatments were performed according to the protocols of Jackson (1985). Original and treated clay-size fractions were used for chemical and macro-XANES analyses.

Table 2 Soil sample nomenclature

Crop rotations	Sampling year, amendment	Name
Continuous corn	2012, unamended	CC/U
	2012, manure	CC/MPS
	2012, unamended before 1954, NPK since 1955	CC/U-NPK
	2012, manure before 1954, NPK since 1955	CC/M-NPK
	1904, unamended	CC/U-1904
Corn-oats-hay	2012, unamended	C-O-H/U
	2012, manure	C-O-H/MPS
	2012, unamended before 1954, NPK since 1955	C-O-H/U-NPK
	2012, manure before 1954, NPK since 1955	C-O-H/M-NPK
	1904, unamended	C-O-H/U-1904

Mineralogical and chemical characterization

XRD analyses of randomly oriented powders prepared from bulk soil samples were performed with a Panalytical X'pert Pro diffractometer equipped with an X'celerator detector using Cu K_α radiation (λ=0.154178 nm) at room humidity (~35 % relative humidity). Diffraction data were recorded from 3 to 64°2θ in a scanning mode and converted to step-scan patterns, with a step of 0.017°2θ and 3 s counting times per step.

Elemental composition (Na, Mg, Al, Si, K, Ca, Ti, Mn, and Fe) was determined by inductively coupled plasma optical emission spectroscopy (ICP-OES) on a Thermo Elemental IRIS instrument after alkali fusion of soils in $LiBO_2$. P concentrations were obtained by ICP-OES on a Agilent 720ES instrument on both bulk soil samples and clay separates following their microwave-assisted digestion in HNO_3/HCl/HF acid (~100 mg samples in 5 mL HNO_3, 2 mL HCl, and 1 mL HF at 200 °C for 18 min). Finally, extractible P was determined using the Bray P1 test (Bray and Kurtz 1945).

Determination of P distribution and speciation using synchrotron radiation

A variety of P-bearing standards was prepared to allow building a limited and specific database for XANES data analysis (Table 3). In particular, NPK fertilizer which is presently applied to the Morrow Plots (13-13-13 Garden Fertilizer Plus Sulfur) was obtained from Estate, P being present as diammonium hydrogen phosphate ($(NH_4)_2HPO_4$). In addition, dissolved organic matter (DOM) was extracted from both Sphagnum and Carex peats, together with their fulvic

Table 3 Standard phosphorus compounds

Inorganic standards		
Name	Formula	Source
Hydroxyapatite	$Ca_5(PO_4)_3(OH)$	Sigma-Aldrich
Na-hexametaphosphate	$(NaPO_3)_n$	Sigma-Aldrich
Hydrated iron phosphate	$Fe(III)PO_4$, $2H_2O$	Sigma-Aldrich
Variscite	$AlPO_4$, $2H_2O$	Muséum National d'Histoire Naturelle (MNHN, Paris), unknown locality (Giguet-Covex et al. 2013)
NPK fertilizer	13-13-13 Garden Ferlilizer Plus Sulfur	Estate
Organic standards		
Name	Formula	Source
Inositol hexakisphosphate (phytic acid Na-salt hydrate)	$C_6H_{18}O_{24}P_6$, xNa^+, yH_2O	Sigma-Aldrich
Adenosine Tri-phosphate (ATP)	$C_{10}H_{16}N_5O_{13}P_3$	Sigma-Aldrich
Dissolved Organic Matter (DOM), fulvic and humic acid fractions		Extracted from Spagnum and Carex peats. Extraction protocols are described in ESM.pdf Online Resource
Sorbed phosphate standards		
Name	Sorption protocol	Source
Phosphate bound to DOM	In ESM.pdf Online Resource	in ESM.pdf Online Resource
Phosphate sorbed onto clay	In ESM.pdf Online Resource	SWy-2 smectite reference from the Source Clay repository was purified as described by Michot et al. (2004)
Phosphate sorbed onto δ-MnO_2	In ESM.pdf Online Resource	δ-MnO_2 was synthesized as described by Villalobos et al. (2003)
Phosphate sorbed onto goethite	Giguet-Covex et al. (2013)	
Phosphate sorbed onto Al oxide		
Phosphate sorbed onto ferrihydrite	Kim et al. (2015)	

and humic acid components (Table 3 and ESM.pdf Online Resource for the protocols). Additional standards were prepared by sorbing P, as phosphate anions, onto mineral soil components (goethite, ferrihydrite, Mn oxide – vernadite, Al oxide, and clays) and by binding these species onto organic soil components (DOM – Table 3 and ESM.pdf Online Resource for the protocols). All samples were finely ground and pressed as pure pellets (P-sorbed soil components, P-bound DOM, bulk soil samples, and fine fractions) or prepared as homogeneous thin films on a P-free adhesive tape (phosphate minerals and commercial organic references).

μ-XRF maps and XANES spectra were collected on the ID21 X-ray microscopy beamline (Salomé et al. 2013) at the European Synchrotron Radiation Facility (ESRF, Grenoble, France). The microscope was operated under vacuum to minimize absorption and scattering by air. The X-ray beam was monochromatized using a fixed-exit double-crystal Si(111) monochromator (0.4 eV resolution). Monochromator energy was calibrated against the first derivative maximum of hydroxyapatite at 2152.0 eV. Flux variations of the incoming beam were corrected by measuring with a photodiode the XRF from a Si_3N_4 (P K-edge) or Ti (Fe K-edge) substrate upstream of the sample. Beam size was reduced using a pinhole (200 μm diameter) for macro-XANES or focused to 0.65×0.25 (h×v) μm^2 with a Kirkpatrick-Baez mirror for μ-XRF and μ-XANES. XRF signal was collected using a 10 mm^2 Röntec or a 80 mm^2 Bruker Si drift diode placed at a 49° angle with respect to sample surface. For standards with high P concentration prepared as thin films on adhesive tape, XANES spectra were collected in transmission mode using a Si diode downstream of the sample. Two-dimensional μ-XRF elemental maps were collected at 2.25 and 7.4 keV (above P and Fe K-edges, respectively), by raster scanning the sample with respect to the X-ray beam. Maps were collected using 100–350 ms data collection times per 0.5–2.0 μm step, depending on P concentration and on the size of P "hot spots". To optimize discrimination of the various XRF line contributions, and specifically to remove Si contribution (originating from quartz and clays) to the P signal, XRF spectra were batch fitted at each map pixel using the PyMCA software (Solé et al. 2007). Spectra fitting relies on Levenberg–Marquardt algorithm and constrained experimental (detectors characteristics, detection geometry, exCitation energy, etc.) and sample (matrix composition) parameters.

P K-edge XANES spectra were collected from 2.13 to 2.20 keV with 0.2 eV energy steps in continuous scan mode. Depending on P concentration and matrix, 2 to 90 quick scan spectra of 0.1 s per energy step were recorded and averaged to optimize signal-to-noise ratio (SNR). No radiation damage was observed during successive data collections. In the present study, self-absorption that can occur during collection of P-rich reference spectra in XRF mode was precluded by collecting data in transmission mode on very thin layers of homogeneous powders. P concentration in sorbed phosphate references and in natural soil samples was low enough not to induce self-absorption effects. XANES spectra were reduced using the standard normalization procedure of the Athena package in Demeter 0.9.20 system (Newville 2001; Ravel and Newville 2005). E_0 edge energy was chosen as the maximum of the data first derivative. Spectra were background corrected using a linear regression fit through the pre-edge region [E_0−22 eV; E_0−8 eV] and a polynomial regression fit through the post-edge region [E_0+28 (+/−3) eV; E_0+42 eV], aiming at a horizontal post-edge signal. Linear combination fittings were performed with Athena over the [E_0−10 eV, E_0+30 eV] range on normalized bulk soil XANES spectra; relative proportions of the components, whose number was limited to four and whose nature was constrained by μ-XANES identification, were forced to sum to 100 %. A precision of ±10 % on the relative proportion of the different contributions is expected from the method (Kelly et al. 2008).

Results

Soil mineralogy and elemental composition

XRD data collected on randomly oriented powders of bulk samples (Fig. ESM1 in ESM.pdf Online Resource) show the common presence of quartz, feldspars (both K-spars and plagioclases), and clay minerals (illite/muscovite, smectite, illite-smectite, kaolinite, and chlorite). P-bearing species are not detected most likely owing to the overall low concentration of P (<0.1 % – Table 4), in addition to a possible crystallinity effect. Relative mineral abundances are similar in the different samples.

Consistent with the prevalence of silicate minerals, soils are dominated by Si (32.7–34.3 wt%; Table 4). Si concentration is higher in non-fertilized soils (U) than in fertilized ones (U-NPK, M-NPK, and MPS),

Table 4 Elemental composition of Morrow plots soil samples (in mg/kg)

Bulk	Continuous Corn (CC)					Corn-Oats-Hay (C-O-H)				
	U	U-NPK	M-NPK	MPS	U-1904	U	U-NPK	M-NPK	MPS	U-1904
Na	6344	6165	6240	6410	n.a.	6388	6158	6069	6180	n.a.
Mg	4607	4963	4902	4649	n.a.	4559	4938	5011	4776	n.a.
Al	52,396	54,688	53,328	50,940	n.a.	51,554	53,052	53,772	52,195	n.a.
Si	342,250	336,966	337,761	340,940	n.a.	343,325	331,309	329,345	326,587	n.a.
K	17,284	16,977	16,885	17,375	n.a.	17,134	16,894	16,918	16,885	n.a.
Ca	4332	5275	5683	5540	n.a.	4761	5354	5618	6097	n.a.
Ti	4400	4406	4442	4346	n.a.	4358	4412	4400	4316	n.a.
Mn	1060	1062	1127	1141	n.a.	1082	1021	965	1065	n.a.
Fe	25,844	27,893	26,942	25,348	n.a.	25,558	26,767	27,578	26,725	n.a.
Total P	354	438	579	589	451	433	591	569	591	455
P in <2 μm fraction	619	749	n.a.	n.a.	n.a.	n.a.	n.a.	n.a.	n.a.	n.a.
P in <2 μm + CBD	225	294	n.a.	n.a.	n.a.	n.a.	n.a.	n.a.	n.a.	n.a.
P in <2 μm + CBD + H_2O_2	102	150	n.a.	n.a.	n.a.	n.a.	n.a.	n.a.	n.a.	n.a.
Exch. P	1.7	24.2	7.4	4.7	n.a.	2.5	22.1	7.3	6.8	n.a.

Note: Exchangeable P (Exch. P) was determined with Bray 1 test. n.a. not analyzed. P in <2 μm fraction of CC/U and CC/U-NPK represent 65 and 64 % of total P, respectively. Standard error on elemental analysis is <2 % for Si and Al, and <5 % for all other elements analysed (<10 % for P concentrations lower than 500 mg/kg)

independent of cropping practices (Table 4). In contrast, Fe concentrations are slightly lower in non-fertilized soils (U) than in fertilized ones (U-NPK, M-NPK, and MPS), but all values remain in a narrow range (2.5–2.8 wt% – Table 4). Consistent with the low pH values [5.4 to 6.5 – Aref and Wander (1998)], low Ca concentrations are measured in soil samples (0.43–0.61 wt%; Table 4), lower concentrations being measured in non-fertilized plots compared to fertilized ones. Concentrations determined for other major elements (Na, Mg, Al, K Ti, and Mn) are essentially independent of fertilizing and cropping practices (Table 4).

As anticipated, fertilizer inputs increase the concentrations of both total and exchangeable P compared to non-fertilized soils (U – Table 4). Specifically, total P concentrations are significantly increased by manure amendments (569–591 mg/kg in M-NPK and MPS subplots compared to 451–455 mg/kg in U-1904 samples). A significant increase of total P concentration is observed for NPK fertilized soils (U-NPK subplots) when compared to present concentrations in unamended subplots (U – Table 4), these concentrations being much lower in CC/U subplot than in C-O-H/U, the latter being similar to total P concentrations in U-1904 samples (Table 4). Among the different fertilizing practices, manure amendments lead to lower concentrations of exchangeable P (4.7–7.5 mg/kg in M-NPK and MPS plots) compared to U-NPK amendments (22–24 mg/kg), however. Reduced P availability in manure-amended soils is consistent with the crystallization of Ca-phosphates from soluble species reported by Sato et al. (2005) for long-term (>25 years) manure application. Available P concentrations are also similar whatever the cropping practices. Finally, P concentrations are increased in the <2 μm clay fraction compared to the bulk sample, independent of amendments (Table 4), the clay fraction, which represents ~35 % of the sample (Odell et al. 1982), accounting for ~65 % of total P.

XANES of bulk samples

XANES spectra of reference compounds As shown in Fig. 1, the energy position of the white line does not vary by more than 1 eV for P species (Brandes et al. 2007; Hesterberg 2010), their differentiation relies mainly on pre-edge features, modulations after the white line, position and shape of the oscillations between 2160 and 2200 eV, and intensity of post-edge features relative to the white line. Sodium hexametaphosphate

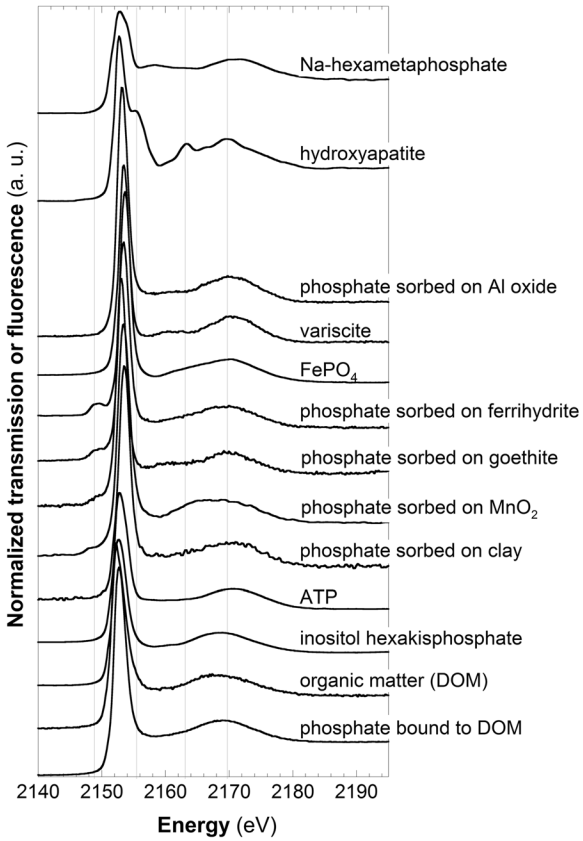

Fig. 1 P K-edge XANES spectra of a selection of reference P minerals, phosphate groups bound to a variety of soil components, and organic species

[$Na_6(PO_3)_6$] presents a broad white line, compared to other species, and two oscillations, a minor one at 2158 eV and a major one centered at 2171 eV. Contrastingly, XANES spectra of calcium phosphates [hydroxy-apatite – $Ca_5(PO_4)_3(OH)$] display three characteristic features: a post-white line shoulder at ~2153 eV and two oscillations at 2161 and 2170 eV (Fig. 1). Although all Ca-phosphate minerals exhibit similar features, the position of the first oscillation and the intensity of the post-white line shoulder and/or of the two oscillations compared to that of the white line may vary as a function of the actual nature of the mineral species (Hesterberg et al. 1999; Beauchemin et al. 2003; Shober et al. 2006; Toor et al. 2006; Ajiboye et al. 2008). This variability can be used to differentiate Ca-phosphate species (Oxmann 2014). In particular, the intensity of the two oscillations is increased compared to that of the white line and the post-white line shoulder is more pronounced and better defined for well-crystallized species [hydroxy-apatite and octacalcium phosphate – $Ca_8H_2(PO_4)_6.5H_2O$] compared to amorphous phosphate varieties (Sato et al. 2005; Güngör et al. 2007; Ingall et al. 2011; Eveborn et al. 2012). When phosphate groups are bound to Fe(III) atoms, such as in [$FePO_4$, $2H_2O$], XANES spectra are characterized by a pre-edge peak at 2149.5 eV (Fig. 1) whose intensity increases with the increasing number of Fe^{3+}-O-P bonds (Khare et al. 2007; Liu and Hesterberg 2011). The systematic presence of this pre-edge peak precludes differentiation of ferric phosphates from phosphates sorbed onto Fe (oxyhydr)oxides, or from Fe-PO_4 co-precipitates (see for example the XANES spectra of [$FePO_4$, $2H_2O$] and of phosphate sorbed onto ferrihydrite – Fig. 1) from their sole XANES fingerprint. Sorption of phosphates onto crystalline iron oxyhydroxides such as goethite [α-FeOOH] induces however a better defined oscillation centered at 2170 eV compared to other Fe-bearing phosphate species (Fig. 1). A pre-edge peak is observed also at ~2148 eV when phosphate groups are bound to Mn(IV) atoms (phosphates sorbed onto vernadite [δ-MnO_2] – Fig. 1).

XANES spectra from phosphate sorbed onto calcite [$CaCO_3$] or co-precipitated with calcite are alike those of poorly crystalline Ca-phosphates, whereas those of phosphate sorbed onto Al oxides resemble those of variscite [$AlPO_4$, $2H_2O$] (Fig. 1) with a constant XRF signal from 2156 to 2164 eV and a broad oscillation centered on 2170.5 eV. Spectra of phosphate sorbed onto clays present also a broad oscillation centered on 2170 eV (Fig. 1), as those of humic-Al-phosphate and humic-montmorillonite-phosphate complexes (Giguet-Covex et al. 2013; Oxmann 2014) and of aqueous phosphate (Güngör et al. 2007; Khare et al. 2007).

XANES spectra of commercial organic phosphates, such as inositol hexakisphosphate and ATP, exhibit no specific fingerprint with a white line at 2152.8 eV and a broad oscillation, whose position and shape depends on the nature of the organic compound (2169 and 2171 eV for inositol phosphate and ATP, respectively – Fig. 1). The spectrum of inositol hexakisphosphate resembles that of P present in natural organic matter (NOM), despite a minor shift of the white line from 2152.8 to 2152.5 eV (Fig. 1). The actual position of the white line depends strongly however both on the origin of the NOM and on the considered fraction (e.g., humic and fulvic acids - Fig. ESM2 in ESM.pdf Online Resource). Additional variability of the white line position is

observed when phosphate is bound to NOM, with a shift of both the white line and the large post-edge oscillation towards higher energies compared to NOM (Fig. ESM2). It should be noted however that the white line is systematically located at lower energy for P bound to NOM than for P sorbed onto soil mineral components (Fig. 1), variation of the white line position being minimal in the latter case. Additional spectra of P-bearing mineral references are available the literature (Franke and Hormes 1995; Brandes et al. 2007; Ingall et al. 2011), whereas more inorganic references can be found in Brandes et al. (2007) and Giguet-Covex et al. (2013).

XANES spectra of bulk soil samples As shown in Fig. 2, XANES spectra collected on soil powders with an unfocused beam systematically show a white line at 2153.2 eV and a broad oscillation at ~2170.5 eV, with no significant variation of the SNR for a similar counting time, consistent with the similar total P concentrations in all samples investigated (Table 4). These spectra strongly differ from that of the NPK fertilizer which exhibits a post-edge shoulder at ~2157 eV and two oscillations at 2162 and 2169 eV (Fig. 2). Rather, the shape of soil spectra closely resembles that of spectra from phosphate bound to NOM or sorbed onto clay minerals, the white line energy position observed on soil samples being intermediate between those of the two reference spectra (inset Fig. 2). When averaging all the XANES spectra collected for the different soil samples in an effort to optimize the SNR and uncover faint features, a minor pre-edge peak is visible at ~2149 eV that is most likely due to phosphate groups bound to Fe atoms.

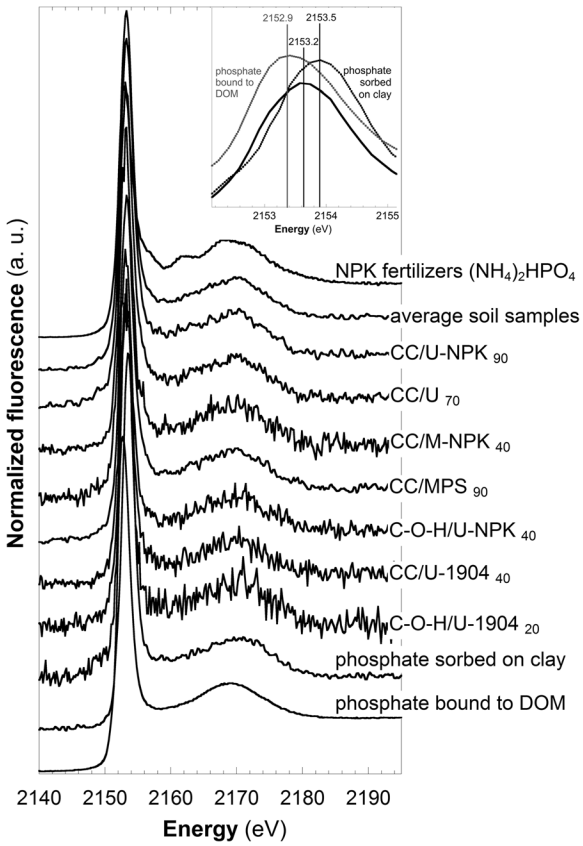

Fig. 2 P K-edge XANES spectra of bulk soil samples from the Morrow plots compared to selected reference spectra. Subscripts following sample names correspond to the number of quick-scan spectra collected and averaged. The inset shows the white line position of the average soil sample spectrum (*solid black line*) compared to that of phosphate groups bound to DOM and sorbed onto clays (*dotted gray* and *black lines*, respectively)

Owing to the increased concentrations of P in the fine size fractions (Table 4), macro-XANES spectra were collected on different clay-size fractions (<2, 0.2–0.05, and <0.05 μm) of CC/U using the same experimental conditions (Fig. 3a). All spectra are alike and resemble those collected on the bulk soil samples with the white line at an intermediate position between phosphate bound to NOM and phosphate sorbed onto clay minerals. The SNR is improved for the <2 μm size fraction compared to the bulk sample, consistent with the higher P concentration in the former sample (Fig. 3a, Table 4). The SNR increases further in 0.2–0.05 and <0.05 μm size fractions (Fig. 3a). On the contrary, this ratio significantly decreases when the <2 μm size fraction is treated with CBD (Fig. 3b), thus supporting bounding of a significant fraction of P to iron (oxyhydr)oxides consistent with the faint pre-edge peak observed on the average bulk soil spectrum. Subsequent removal of organic matter with H_2O_2 decreases further the SNR (Fig. 3b), suggesting that part of the remaining P is bound to the organic fraction either as organic P species or as phosphate bound to organic matter. In both cases, decrease of the SNR is consistent with the lower P concentrations measured in the CBD treated and further in the CBD-H_2O_2-treated fractions compared to the untreated <2 μm fraction (Table 4). Finally, it should be noted that the position of the white line appears, within error due to low counting statistics, as independent of the considered size fraction and does not vary either upon subsequent treatments of the clay-size fractions.

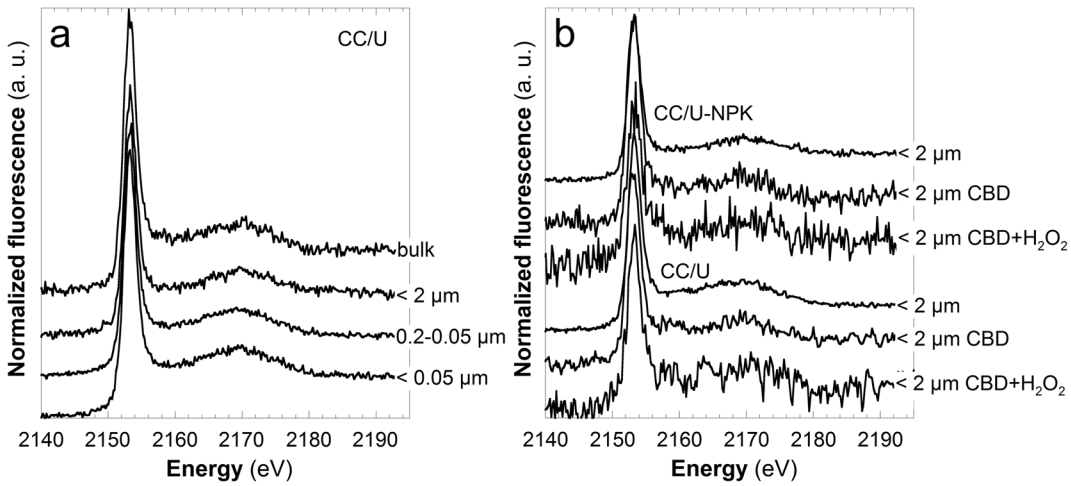

Fig. 3 P K-edge XANES spectra of the soil clay-size fraction. **a**) Comparison of the XANES spectra collected on the <2, 0.2–0.05, and <0.05 µm fractions of CC/U with that obtained on the bulk soil (systematic collections of 50 quick-scan spectra). **b**) Comparison of the XANES spectra collected on the <2 µm fractions of CC/U-NPK (*top*, 50 quick-scan spectra) and CC/U (*bottom*, 40 quick-scan spectra) before and after CBD and H_2O_2 treatments

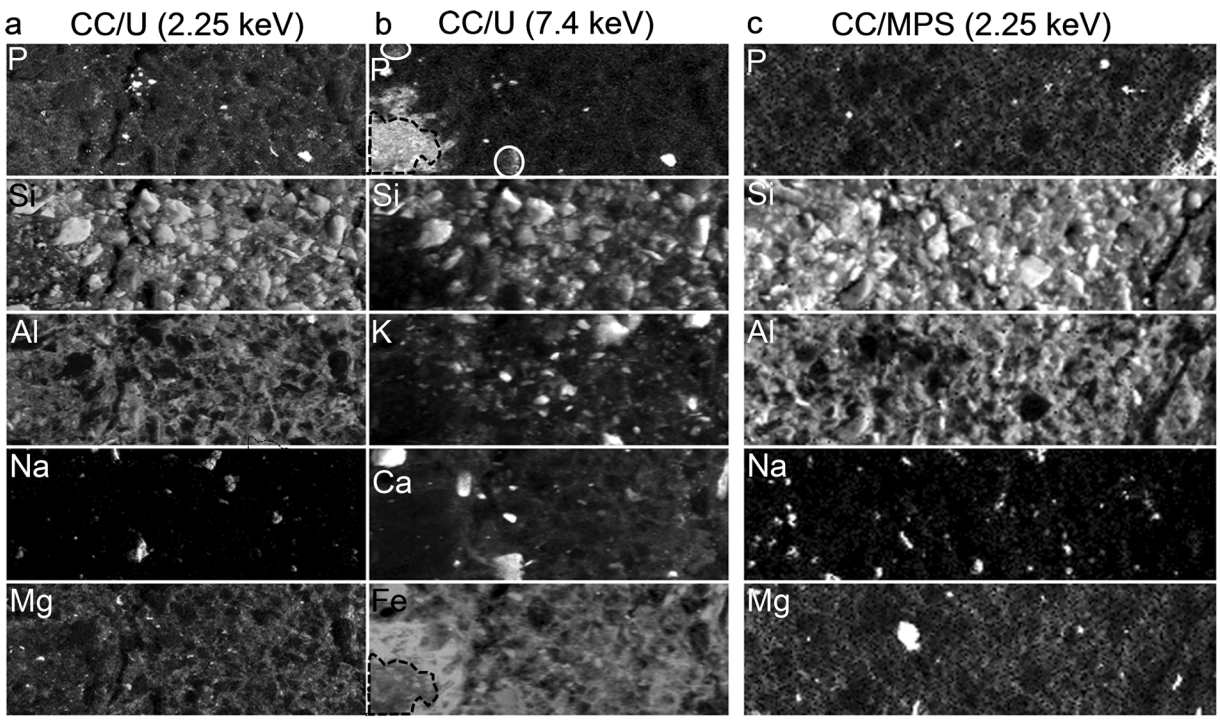

Fig. 4 µ-XRF maps of CC/U (**a** and **b**) and CC/MPS (**c**) collected at 2.25 (**a** and **c**) and 7.4 (**b**) keV showing P, Si, Al, Na, Mg, K, Ca and Fe distributions as gray-scale images (light represents high counts, dark low counts). The areas mapped are 300 × 120 and 400 × 120 µm^2 for CC/U and CC/MPS, respectively. The P-rich area at the bottom right of CC/MPS map is a root section. Ellipses and dotted line delimit areas where the X-ray detector saturates due to high concentration of Ca and Fe, respectively. As a result, the concentration of P is artificially increased in these areas. *Color figure* is available in ESM.pdf online resource (Fig. ESM3)

Laterally-resolved XRF and XANES

Distribution of P in soils at the micrometer scale μ-XRF maps were collected on thin sections of CC/U (Fig. 4 left, Fig. ESM3 in ESM.pdf Online Resource), CC/U-NPK, CC/MPS (Fig. 4 right, Fig. ESM3), C-O-H/U, and C-O-H/U-NPK above P K-edge and on thin sections of CC/U (Fig. 4 middle), CC/U-NPK, and C-O-H/U-NPK above Fe K-edge to determine elemental distribution in undisturbed soil samples. The P maps systematically show the presence of minute (~2 to 50 μm) hot spots disseminated in a low-concentration diffuse background (bright spots and gray background, respectively, in Fig. 4 top). Within this background, areas devoid of quartz grains (bottom left of Si map in Fig. 4a) appear enriched in P compared to the rest of the map, possibly as the result of a reduced dilution by unreactive quartz grains. No significant difference is observed between the P distributions from different samples or as a function of cropping and fertilizing practices. Correlation of P hot spots with Ca is observed occasionally whereas no significant correlation with lighter element (Si, Al, Mg, or Na) is evidenced (Fig. 4, Fig. ESM3, R^2=5 % on selected hotspots). Similarly, no significant correlation is observed between Al and P concentrations in areas devoid of quartz grains (e.g., lower left corner of Fig. 4a, Fig. ESM3, R^2=2 %) but a correlation is observed between P and Fe in these areas (RGB P-Fe-Ca map in Fig. ESM3). Finally, P fluorescence yield and thus concentration appears unchanged in areas vicinal to roots (lower right corner of maps in Fig. 4c).

μ-XANES spectra at selected points of interest 10–25 XANES spectra were collected at specific points of interest (POIs) on thin sections of CC/U, CC/U-NPK, CC/MPS, C-O-H/U, and C-O-H/U-NPK to assess the heterogeneity of P speciation (Fig. 5). One to three of these spectra originate from apatitic species in CC/U-NPK, C-O-H/U and C-O-H/U-NPK, corresponding POIs being systematically P hot spots whose size varies from <5 to ~50 μm. Other spectra collected at hot spots in CC/U evidenced a slight shift of their white line towards lower energy compared to spectra of phosphate sorbed onto Al- and Fe-phosphates and broad oscillations at ~2158 and ~2171 eV (Fig. 5, non attributed spectrum). These hot spots do not evidence any correlation with elements mapped at the P K-edge but local correlations with Ca are noticeable (Fig. 4 and

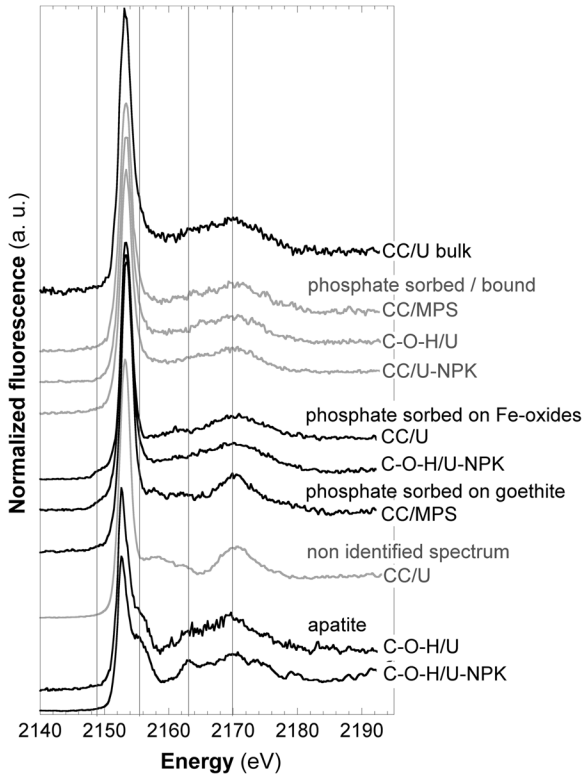

Fig. 5 Selection of P K-edge μ-XANES spectra collected at specific points of interest on CC/U, CC/U-NPK, CC/MPS, C-O-H/U, and C-O-H/U-NPK and comparison with CC/U bulk spectrum

Fig. ESM3). Corresponding XANES spectra do not match those of mineral references from or outside the apatite group (Ingall et al. 2011) and actual nature of these species remains uncertain. Spectra corresponding to phosphate sorbed onto goethite and on unidentified iron (oxyhydr)oxides are observed in CC/U, CC/MPS and C-O-H/U-NPK. These spectra were collected at high-Fe and low-P POIs (lower intensity than apatite hot-spots) or as part of the low-P concentration background,inconsistent with structural P in Fe-phosphates, despite spectral similarities. Most other spectra were similar to the bulk spectra (Fig. 5), with a slight shift of the white line by up to 0.2 eV compared to the bulk spectra. The white line remains systematically located at an energy intermediate between those of phosphate bound to natural organic matter and phosphate sorbed onto clay minerals, however, thus pleading for an intimate association of P with clay-humus complexes.

Discussion

P speciation in agricultural soils from the Morrow plots

In addition to the white line, XANES spectra collected at the P K-edge on bulk soil samples systematically exhibit a unique broad modulation centered at ~2170 eV (Fig. 2). Such XANES spectra differ significantly from the XANES fingerprint of NPK fertilizers that are presently used to amend the Morrow Plots. The low persistence of the initial P form [diammonium hydrogen phosphate, $(NH_4)_2HPO_4$] is consistent with the high solubility of the P input required by its short-term availability and this compound is not detected when fitting the average spectrum obtained by summing up all spectra collected on bulk soil samples from individual plots (Fig. 6). Three major standard contributions are used to fit this average spectrum: phosphate bound to DOM from sphagnum peat represents 33–44 % of total P, whereas phosphate sorbed onto Fe-oxides and P present in DOM from sphagnum peat account for 37–44 and 15–23 % of total P, respectively (Fig. 6). The best fit to the XANES data includes the presence of P sorbed onto both ferrihydrite (31 %) and goethite (13 % – Fig. 6a). A fit of similar quality (R-factor = 0.0023 in both cases) is obtained with ferrihydrite as the sole Fe-oxide sorbent (37 %) and a minor hydroxyapatite contribution (4 % of total P – Fig. 6b), the latter contribution being lower than the precision expected from the method, however [~10 % – Kelly et al. (2008)]. The best fit that includes a contribution of phosphate sorbed onto Al oxide is slightly degraded compared to the two optimum fits (R-factor 0.0024 – Fig. ESM4 in ESM.pdf Online Resource). In addition, the contribution of phosphate sorbed onto Al oxide (6 % of total P) remains below the actual sensitivity of the method whereas other contributions are akin those in the optimum fits (phosphate bound to DOM: 35 %, phosphate sorbed onto Fe-oxide: 37 %, and DOM: 22 %). XANES data may be fitted also assuming a contribution of phosphate sorbed onto clays but significant discrepancies are visible over the pre-edge region (R-factor = 0.0026 – Fig. ESM4) owing to specific spectral fingerprint of phosphate bound to Fe(III) or Mn(IV) (not included in the fit owing to the low Mn content) atoms. P speciation is thus dominated by phosphate bound to fine-grained soil components, consistent with previous reports (Ajiboye et al. 2008). Relative proportions of organic (~60 %) and mineral (~40 %) sorbents depend primarily on the actual position of the white line which differs significantly for the two main contributions. The actual nature of phosphate groups involved (e.g. their protonation state and charge) remains poorly constrained however, together with the actual binding configuration to the different soil components. Influence of soil pH and base cation composition on P binding configuration and more globally on P speciation also remains to be determined.

In addition to the main P-bearing components identified from macro-XANES analysis of bulk samples, analyses performed with a sub-micron beam on thin sections indicate the presence of "hot spots" mainly composed of apatitic species. Despite their spectral similarity with polyphosphates and previous reports of their presence in agricultural soils (Beauchemin et al. 2003; Eriksson et al. 2015), no Al phosphate or phosphate sorbed onto Al (oxyhydr)oxides were identified in the sample as no Al was detected by

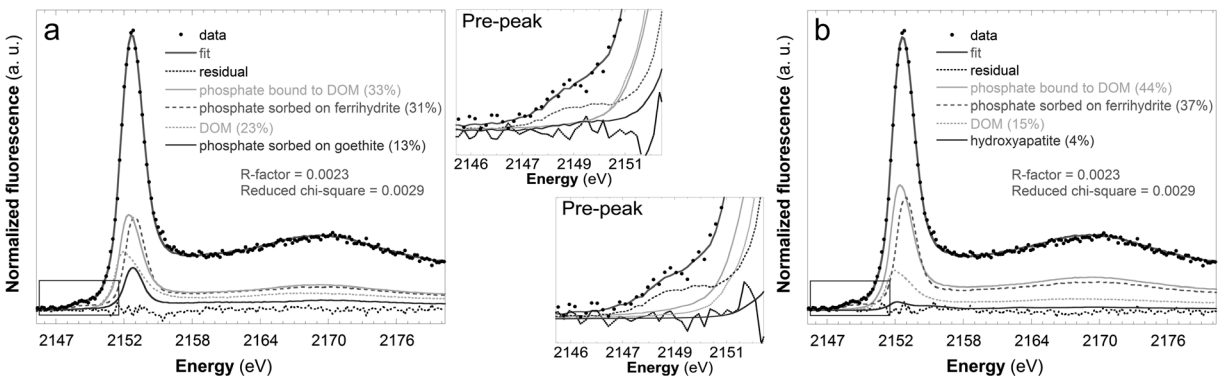

Fig. 6 Average P K-edge XANES spectrum of the Morrow plots bulk soil (*dots*) and best (**a**) and second best (**b**) linear combination fits (*solid gray line*) with four components. Insets zoom on the pre-edge regions of the two fits. DOM is the bulk DOM from Sphagnum peat

μ-XRF at P hot spots, thus excluding association of phosphate to Al–rich minerals. Despite their high-intensity XRF signal, phases detected at P "hot spots" remain extremely localized and their contribution to the overall P speciation is insignificant. Bulk P XANES signal thus comes essentially from the low and diffuse background observed on the μ-XRF maps of P and not from the hot spots. No significant modification of this average signal or of P XRF signal (Fig. 4c) is observed in the vicinity of roots, despite previous reports in the literature. Hinsinger (2001) describes for example modifications of P concentration and availability in the rhizosphere as the result of local pH modification or of organic acids/anions exudation.

The association of P with soil fined grained components is consistent with its enrichment in the clay-size fraction (Table 4) which accounts for ~65 % of total P, although it represents ~35 % of the soil (Odell et al. 1982), and with previous reports (Williams and Saunders 1956; Pierzynski et al. 1990). After CBD treatment of the clay-size fraction, P concentration is reduced by ~2/3, thus suggesting prevalence of P bound to finely divided Fe oxides, although XANES spectra exhibit only a weak pre-edge peak and ~40 % contribution of P sorbed onto Fe oxides. This discrepancy may be concealed by considering the role of Fe oxides as a cement of the organo-mineral complexes, in addition to the limited selectivity of CBD for Fe oxides (Jackson 1985; Varadachari et al. 2006). As a consequence of the complex breakdown, removal of Fe oxides releases into solution P actually bound to Fe oxides but also P bound to extremely fine grained material, and more especially to clays and organic matter, which contain most of P either as bound complexes or within its own structure (DOM). Further decrease of P concentration upon H_2O_2 treatment supports further the association of P with organo-mineral complexes, in agreement with previous reports on soils and young sediments (Giguet-Covex et al. 2013). This association is consistent also with the constant spectral signature observed both at the macro and sub-micron scales, with no incidence of elementary spectra corresponding to pure end-member contributions. Further support to this association arises from the similarity of P XANES spectra recorded on different clay-size fractions (Fig. 3a) and on the <2 μm fraction both untreated and after the different chemical treatments (Fig. 3b). The actual nature of natural organic matter controls both its intrinsic P K-edge XANES spectral fingerprint, and more especially the position of the white line, and the spectral fingerprint of bound phosphate groups (Fig. ESM2 in ESM.pdf Online Resource). Although limited, this sensitivity stresses the need for appropriate organic references in the determination of P speciation in soils and sediments and thus for a large database of references based on natural organic matter. Solid-state ^{31}P NMR thus appears as an interesting complementary method owing to its enhanced sensitivity to subtle differences in the organic matter compared to XANES (Doolette and Smernik 2011).

Finally, spectra collected on samples from the different plots are all alike (Fig. 2), thus pleading for a minor effect of both cropping and fertilizing practices on P speciation. P distribution (Fig. 4c) and speciation (not shown) is similar also in root vicinity, bringing additional support to a limited effect of cropping practices. On a longer perspective, the similarity of XANES spectra collected at the P K-edge on present day samples and on samples from U-1904 pleads also for a limited impact of cropping and fertilizing practices on P speciation. If the status of soil P appears constant, the total concentration of P depends on cropping and fertilizing practices (Table 4) with increases by ~30 % of the total P reservoir in CC/M-NPK, CC/MPS and C-O-H/NPK, C-O-H/M-NPK, and C-O-H/MPS compared to their U-1904 equivalents (CC/U-1904 and C-O-H/U-1904, respectively). Total soil P concentration decreases only in CC/U (by ~20 %), whereas concentrations similar to those in U-1904 samples were determined in plots CC/U-NPK and C-O-H/U.

Distribution of P-bearing species in undisturbed soil samples with μ-XRF and μ-XANES

Although P distribution in soils is dominated by a low-concentration diffuse background, the presence of minute hot spots requires using a high-resolution and high-sensitivity mapping to uncover a complete description of P speciation in heterogeneous systems such as soils and fine-grained sediments. The X-ray microscope available at ID21 allows collecting XRF maps and XANES spectra at a sub-micron resolution (0.65 × 0.25 μm^2) for P concentrations as low as a few hundreds ppm. Lateral resolution allows probing specific areas such soil-root interfaces, in terms of elemental distribution and speciation.

The counterpart of observations performed at the sub-micron scale on large heterogeneous samples is their limited representativity, especially as limited

access to well-suited synchrotron beamlines may impede acquisition of multiple μ-XRF maps and of μ-XANES spectra on multiple low-concentration POIs. In addition, human eye is intuitively attracted by hot spots brightness and data is likely collected preferentially at these points, compared to low-intensity background. As a consequence, the number of elementary spectra collected for each specific type is most likely biased, especially when the number of μ-XANES spectra collected for a given sample is low. The information obtained fom μ-XRF and μ-XANES can be key to uncover minor contributions to the bulk XANES signature of the element considered. In addition, and despite the limited representativity, μ-XRF analyses can provide information on the size distribution of P-bearing particles and their spatial distribution in undisturbed samples.

The low number of synchrotron beamlines optimized to work at the P K-edge (~2.15 keV) dramatically reduces the present feasibility of such investigations, in addition to limitations in terms of data collection and processing (Hesterberg 2010). In addition, the limited contrast of XANES spectra at the P K-edge remains a key issue for investigating P speciation as shown by the similar spectra obtained from a variety of reference spectra: amorphous apatite and phosphate sorbed onto calcite, iron phosphate and phosphate sorbed onto iron oxides. In such cases, XRF and XANES data collection at other edges (Fe, Ca, Mn, or Al K-edges) can efficiently eliminate ambiguity. Finally, P in a variety of organic compounds (ATP, inositol, …) exhibit spectra similar to those from phosphate groups bound to a variety of sorbents (organic matter, clays, e.g.). In this case, the position of the white line varies by less than 1 eV. The theoretical resolution (0.4 eV at 2.15 keV), stability, and reproducibility of ID21 monochromator allows differentiating reference spectra with such limited contrast, and represents a major improvement compared to previous studies (Brandes et al. 2007). The white line of organic P and of phosphate groups bound to organic matter consistently occurs at 2152.8–2152.9 eV, whereas phosphate groups sorbed onto mineral references occurs at 2153.4–2153.6 eV, when no post-edge shoulder is present. In the present study, P white line was systematically located at a constant intermediate position between those of phosphate bound to natural organic matter and of phosphate sorbed onto clay minerals (Fig. 2, inset), thus pleading for the systematic association of P with clay-humic complexes. Subtle but significant differences in the position and shape of XANES spectra of phosphate bound to different natural organic matter standards (Fig. ESM2b in ESM.pdf Online Resource) stress however the need for a careful characterization of the organic sorbent.

Acknowledgments The kind help of Michelle M. Wander (Dpt. Natural Resources and Environmental Sciences, Univ. of Illinois, Urbana-Champaign campus) during field-sampling and archive search is gratefully acknowledged. Martine Lanson (ISTerre, Grenoble, France) is thanked for analyses of total P, organic matter extraction and fractionation, and technical assistance for sorption experiments. Bernard Martin (EPOC, Bordeaux, France) is thanked for the preparation of the petrographic micro-polished thin sections. ICP-OES analyses were performed at the Service d'Analyse des Roches et des Minéraux (SARM-CNRS, Vandoeuvre-lès-Nancy, France) for major elements and at the Centre de Coopération Internationale en Recherche Agronomique pour le Développement (CIRAD, Montpellier, France) for extractible P (Bray test). Synchrotron analyses were conducted on the ID21 beamline at the European Synchrotron Radiation Facility (Grenoble, France) on in-house research beamtime. This work has been supported by a grant from Labex OSUG@2020 (Investissements d'avenir – ANR10 LABX56).

References

Abdala DB, da Silva IR, Vergütz L, Sparks DL (2015) Long-term manure application effects on phosphorus speciation, kinetics and distribution in highly weathered agricultural soils. Chemosphere 119:504–514. doi:10.1016/j.chemosphere.2014.07.029

Ajiboye B, Akinremi OO, Hu Y, Jurgensen A (2008) XANES speciation of phosphorus in organically amended and fertilized vertisol and mollisol. Soil Sci Soc Am J 72:1256–1262. doi:10.2136/sssaj2007.0078

Aref S, Wander MM (1998) Long-term trends of corn yield and soil organic matter in different crop sequences and soil fertility treatments on the Morrow Plots. Adv Agron 62:153–197. doi:10.1016/S0065-2113(08)60568-4

Beauchemin S, Hesterberg D, Chou J, Beauchemin M, Simard RR, Sayers DE (2003) Speciation of phosphorus in phosphorus-enriched agricultural soils using X-ray absorption near-edge structure spectroscopy and chemical fractionation. J Environ Qual 32:1809–1819. doi:10.2134/jeq2003.1809

Brandes JA, Ingall E, Paterson D (2007) Characterization of minerals and organic phosphorus species in marine sediments using soft X-ray fluorescence spectromicroscopy. Mar Chem 103:250–265. doi:10.1016/j.marchem.2006.09.004

Bray RH, Kurtz LT (1945) Determination of total, organic, and available forms of phosphorus in soils. Soil Sci 59:39–45. doi:10.1097/00010694-194501000-00006

Cade-Menun BJ (2005) Characterizing phosphorus in environmental and agricultural samples by ^{31}P nuclear magnetic

resonance spectroscopy. Talanta 66:359–371. doi:10.1016/j.talanta.2004.12.024
Chang SC, Jackson ML (1957) Fractionation of soil phosphorus. Soil Sci 84:133–134
Doolette AL, Smernik RJ (2011) Soil organic phosphorus speciation using spectroscopic techniques. In: Bünemann E, Oberson A, Frossard E (eds) Phosphorus in action, vol 26. Springer, New York, pp 3–36. doi:10.1007/978-3-642-15271-9_1
Eriksson AK, Gustafsson JP, Hesterberg D (2015) Phosphorus speciation of clay fractions from long-term fertility experiments in Sweden. Geoderma 241–242:68–74. doi:10.1016/j.geoderma.2014.10.023
Eveborn D, Kong D, Gustafsson JP (2012) Wastewater treatment by soil infiltration: long-term phosphorus removal. J Contam Hydrol 140–141:24–33. doi:10.1016/j.jconhyd.2012.08.003
Franke R, Hormes J (1995) The P K-near edge absorption spectra of phosphates. Physica B 216:85–95
Giguet-Covex C, Poulenard J, Chalmin E, Arnaud F, Rivard C, Jenny JP, Dorioz JM (2013) XANES spectroscopy as a tool to trace phosphorus transformation during soil genesis and mountain ecosystem development from lake sediments. Geochim Cosmochim Acta 118:129–147
Güngör K, Jürgensen A, Karthikeyan KG (2007) Determination of phosphorus speciation in dairy manure using XRD and XANES spectroscopy. J Environ Qual 36:1856–1863. doi:10.2134/jeq2006.0563
Hedley MJ, Stewart JWB, Chauhan BS (1982) Changes in inorganic and organic soil phosphorus fractions induced by cultivation practices and by laboratory incubations. Soil Sci Soc Am J 46:337–347
Hesterberg D (2010) Macroscale chemical properties and X-ray absorption spectroscopy of soil phosphorus. In: Balwant S, Markus G (eds) Developments in soil science, vol 34. Elsevier, New York, pp 313–356. doi:10.1016/S0166-2481(10)34011-6
Hesterberg D, Zhou WQ, Hutchison KJ, Beauchemin S, Sayers DE (1999) XAFS study of adsorbed and mineral forms of phosphate. J Synchrotron Radiat 6:636–638
Hinsinger P (2001) Bioavailability of soil inorganic P in the rhizosphere as affected by root-induced chemical changes: a review. Plant Soil 237:173–195. doi:10.1023/A:1013351617532
Ingall ED, Brandes JA, Diaz JM, de Jonge MD, Paterson D, McNulty I, Elliott WC, Northrup P (2011) Phosphorus K-edge XANES spectroscopy of mineral standards. J Synchrotron Radiat 18:189–197. doi:10.1107/S0909049510045322
Irving GCJ, McLaughlin MJ (1990) A rapid and simple field-test for phosphorus in Olsen and Bray N°1 extracts of soil. Commun Soil Sci Plant Anal 21:2245–2255. doi:10.1080/00103629009368377
Jackson ML (1985) Soil chemical analysis - Advanced course. 2nd Edition, 11th printing published by the author, Madison WI
Kar G, Peak D, Schoenau JJ (2012) Spatial and chemical speciation of soil phosphorus in a band application. Soil Sci Soc Am J 76:2297–2306. doi:10.2136/sssaj2012.0146
Kelly S, Hesterberg D, Ravel B (2008) Analysis of soils and minerals using X-ray absorption spectroscopy. In: Ulery A, Drees L (eds) Methods of soil analysis, vol 5, Part 5: mineralogical methods. Soil Science Society of America, Madison, pp 387–463
Khare N, Martin JD, Hesterberg D (2007) Phosphate bonding configuration on ferrihydrite based on molecular orbital calculations and XANES fingerprinting. Geochim Cosmochim Acta 71:4405–4415
Kim B, Gautier M, Rivard C, Sanglar C, Michel P, Gourdon R (2015) Effect of aging on phosphorus speciation in surface deposit of a vertical flow constructed wetland. Environ Sci Technol 49: 4903–4910. doi:10.1021/es506164v
Kruse J, Leinweber P (2008) Phosphorus in sequentially extracted fen peat soils: a K-edge X-ray absorption near-edge structure (XANES) spectroscopy study. J Plant Nutr Soil Sci 171:613–620. doi:10.1002/jpln.200700237
Kruse J, Abraham M, Amelung W, Baum C, Bol R, Kühn O, Lewandowski H, Niederberger J, Oelmann Y, Rüger C, Santner J, Siebers M, Siebers N, Spohn M, Vestergren J, Vogts A, Leinweber P (2015) Innovative methods in soil phosphorus research: a review. J Plant Nutr Soil Sci 178:43–88. doi:10.1002/jpln.201400327
Liu Y-T, Hesterberg D (2011) Phosphate bonding on noncrystalline Al/Fe-hydroxide coprecipitates. Environ Sci Technol 45:6283–6289
Liu J, Yang J, Cade-Menun BJ, Liang X, Hu Y, Liu CW, Zhao Y, Li L, Shi J (2013) Complementary phosphorus speciation in agricultural soils by sequential fractionation, solution ^{31}P nuclear magnetic resonance, and phosphorus K-edge X-ray absorption near-edge structure spectroscopy. J Environ Qual 42:1763–1770. doi:10.2134/jeq2013.04.0127
Lombi E, Susini J (2009) Synchrotron-based techniques for plant and soil science: opportunities, challenges and future perspectives. Plant Soil 320:1–35. doi:10.1007/s11104-008-9876-x
Lombi E, Scheckel KG, Armstrong RD, Forrester S, Cutler JN, Paterson D (2006) Speciation and distribution of phosphorus in a fertilized soil: a synchrotron-based investigation. Soil Sci Soc Am J 70:2038–2048. doi:10.2136/sssaj2006.0051
Lookman R, Geerts H, Grobet P, Merckx R, Vlassak K (1996) Phosphate speciation in excessively fertilized soil: a ^{31}P and ^{27}Al MAS NMR spectroscopic study. Eur J Soil Sci 47:125–130
Matejovic I, Durackova A (1994) Comparison of mehlich 1-, 2-, and 3-, calcium chloride-, bray-, olsen-, enger-, and schachtschabel-extractants for determinations of nutrients in two soil types. Commun Soil Sci Plant Anal 25:1289–1302. doi:10.1080/00103629409369115
McDowell RW, Condron LM, Mahieu N, Brookes PC, Poulton PR, Sharpley AN (2002) Analysis of potentially mobile phosphorus in arable soils using solid state nuclear magnetic resonance. J Environ Qual 31:450–456. doi:10.2134/jeq2002.4500
Michot LJ, Bihannic I, Porsch K, Maddi S, Baravian C, Mougel J, Levitz P (2004) Phase diagrams of Wyoming Na-montmorillonite clay. Influence of particle anisotropy. Langmuir 20:10829–10837. doi:10.1021/la0489108
Negassa W, Kruse J, Michalik D, Appathurai N, Zuin L, Leinweber P (2010) Phosphorus speciation in agro-industrial byproducts: sequential fractionation, solution ^{31}P NMR, and P K- and $L_{2,3}$-Edge XANES spectroscopy. Environ Sci Technol 44:2092–2097. doi:10.1021/es902963c

Newville M (2001) IFEFFIT: interactive XAFS analysis and FEFF fitting. J Synchrotron Radiat 8:322–324. doi:10.1107/S0909049500016964

Odell RT, Walker WM, Boone LV, Oldham MG (1982) The morrow plots: a century of learning. Agricultural Experiment Station, College of Agriculture, Univ. of Illinois, Urbana-Champaign

Oxmann JF (2014) Technical Note: an X-ray absorption method for the identification of calcium phosphate species using peak-height ratios. Biogeosciences 11:2169–2183. doi:10.5194/bg-11-2169-2014

Oxmann JF, Pham QH, Lara RJ (2008) Quantification of individual phosphorus species in sediment: a sequential conversion and extraction method. Eur J Soil Sci 59:1177–1190. doi:10.1111/j.1365-2389.2008.01062.x

Peak D, Sims JT, Sparks DL (2002) Solid-state speciation of natural and alum-amended poultry litter using XANES spectroscopy. Environ Sci Technol 36:4253–4261. doi:10.1021/es025660d

Peak D, Kar G, Hundal L, Schoenau J (2012) Kinetics and mechanisms of phosphorus release in a soil amended with biosolids or inorganic fertilizer. Soil Sci 177:183–187, 110.1097/SS.1090b1013e31823fd31478

Pierzynski GM, Logan TJ, Traina SJ, Bigham JM (1990) Phosphorus chemistry and mineralogy in excessively fertilized soils: quantitative analysis of phosphorus-rich particles. Soil Sci Soc Am J 54:1576–1583. doi:10.2136/sssaj1990.03615995005400060011x

Prietzel J, Dümig A, Wu Y, Zhou J, Klysubun W (2013) Synchrotron-based P K-edge XANES spectroscopy reveals rapid changes of phosphorus speciation in the topsoil of two glacier foreland chronosequences. Geochim Cosmochim Acta 108:154–171. doi:10.1016/j.gca.2013.01.029

Ravel B, Newville M (2005) ATHENA, ARTEMIS, HEPH AESTUS: data analysis for X-ray absorption spectroscopy using IFEFFIT. J Synchrotron Radiat 12:537–541

Ruban V, López-Sánchez J, Pardo P, Rauret G, Muntau H, Quevauviller P (1999) Selection and evaluation of sequential extraction procedures for the determination of phosphorus forms in lake sediment. J Environ Monit 1:51–56

Salomé M, Cotte M, Baker R, Barrett R, Benseny-Cases N, Berruyer G, Bugnazet D, Cornu HC-M, Fayard B, Gagliardini E, Hino R, Morse J, Papillon E, Pouyet E, Rivard C, Solé VA, Susini J, Veronesi G (2013) The ID21 scanning X-ray microscope at ESRF. J Phys Conf Ser 425:182004. doi:10.1088/1742-6596/425/18/182004

Sato S, Solomon D, Hyland C, Ketterings QM, Lehmann J (2005) Phosphorus speciation in manure and manure-amended soils using XANES spectroscopy. Environ Sci Technol 39:7485–7491

Shober AL, Hesterberg DL, Sims JT, Gardner S (2006) Characterization of phosphorus species in biosolids and manures using XANES spectroscopy. J Environ Qual 35:1983–1993. doi:10.2134/jeq2006.0100

Solé VA, Papillon E, Cotte M, Walter P, Susini J (2007) A multiplatform code for the analysis of energy-dispersive X-ray fluorescence spectra. Spectrochim Acta B 62:63–68. doi:10.1016/j.sab.2006.12.002

Tiyapongpattana W, Pongsakul P, Shiowatana J, Nacapricha D (2004) Sequential extraction of phosphorus in soil and sediment using a continuous-flow system. Talanta 62:765–771. doi:10.1016/j.talanta.2003.09.018

Toor GS, Hunger S, Peak JD, Sims JT, Sparks DL (2006) Advances in the characterization of phosphorus in organic wastes: environmental and agronomic applications. Adv Agron 89:1–72

Varadachari C, Goswani G, Ghosh K (2006) Dissolution of iron oxides. Clay Res 25:1–19

Villalobos M, Toner B, Bargar J, Sposito G (2003) Characterization of the manganese oxide produced by *pseudomonas putida* strain MnB1. Geochim Cosmochim Acta 67:2649–2662. doi:10.1016/S0016-7037(03)00217-5

Wang C, Zhang Y, Li H, Morrison RJ (2013) Sequential extraction procedures for the determination of phosphorus forms in sediment. Limnology 14:147–157. doi:10.1007/s10201-012-0397-1

Williams EG, Saunders WMH (1956) Distribution of phosphorus in profiles and particle-size fractions of some scottish soils. J Soil Sci 7:90–109. doi:10.1111/j.1365-2389.1956.tb00866.x